Impact of fluoride concentration on general corrosion of Mg-Zr alloy in a Na-geopolymer and alkaline solutions

C.F. Barros, B. Muzeau, V. L'hostis, Raoul François

Version of Record: https://www.sciencedirect.com/science/article/pii/S0010938X19326071
Manuscript_33168fd1ae8a6482a0876d081790a2c4

Impact of fluoride concentration on general corrosion of Mg-Zr alloy in a Na-geopolymer and alkaline solutions

C. F. Barros[1], B. Muzeau[1], V. L'Hostis[1], R. François[2]

[1]*Den-Service d'Etude du Comportement des Radionucléides (SECR), CEA, Université Paris-Saclay, 91191 Gif-sur-Yvette, France*

[2] *LMDC, INSA, UPS, Université de Toulouse, France*

Abstract

Corrosion of a metal in cementitious media can be limited when the pore solution of the binder contains corrosion inhibitors, as in the case of immobilization of magnesium nuclear wastes in France. This works aims to elucidate the impact of NaF on the magnesium corrosion, when it is incorporated in the Na-geopolymer formulation. The presence of NaF, even in small concentrations, considerably reduces the amount of corrosion products found on the magnesium/Na-geopolymer interface. Some concentration ranges were considered optimal for reducing corrosion and are related to the type of corrosion film formed on the metal surface, which provides greater protection.

Highlights

- Impact of fluoride concentration on the corrosion rate of magnesium in alkaline solutions and in Na-geopolymer.
- NaF concentration ranges required to reduce corrosion in alkaline solutions and in Na-geopolymer.
- Morphology and chemical composition of corrosion products formed on magnesium surface.
- Proposition of corrosion mechanisms in presence of fluoride in Na-geopolymer and in alkaline media.

Keywords: magnesium, polarization, alkaline corrosion, anodic films.

Introduction

Magnesium alloys are known for their reactivity and their corrosion is commonly associated with hydrogen releases. Reducing the corrosion rate of these alloys and consequently the hydrogen evolution is essential in some situations, such as the storage of metallic wastes from the UNGG (Uranium Natural Graphite Gas) nuclear reactors. Preliminary studies pointed out Na-geopolymers containing NaF as the most adapted materials for the immobilization of magnesium wastes due to their low corrosion rate and low hydrogen evolution [1,2].

The geopolymer provides physical and chemical protection for magnesium. It acts as a physical barrier that minimizes contact between the metal and the external environment. Nevertheless, corrosion of magnesium alloys could occur in the geopolymer due electrochemical reactions with the pore solution of the cementitious matrix, and then reduce the protective effect. There are indications that the uniform corrosion process in Na-geopolymer/NaF is limited by the presence of fluoride ions in its pore solution [2], due to their ability to inhibit the magnesium corrosion [3–7]. However, divergences are listed for the optimal concentration required to obtain the lowest corrosion rate [3,5,8–10]. This phenomenon can be correlated to the structure of the corrosion products formed on the

metal/matrix interface, which is directly proportional to the fluoride concentration in the pore solution.

Predicting variations of the fluoride concentration in geopolymer pore solutions is relevant since they depend on the interactions between the liquid and solid phases, as well as their ability to diffuse through the hydraulic binder to reach the metal surface during the corrosion/inhibition process. As the concentration of fluoride may vary, corrosion is subject to modification and this mechanism must be further investigated.

A common method used to study corrosion in a cementitious matrix consists in performing tests directly in the pore solution extracted from the cement paste, or in solutions representative of the interstitial solution [11–13]. The preference for the study in solution is due to its simple setup and interpretation, in contrast to studies conducted in hydraulic binders. Nevertheless, a part of this study was conducted in geopolymer mortars, to compare the responses with the ones obtained in simulated pore solution.

This work aims to understand the general corrosion of magnesium in the presence of fluoride and how its concentration can affect the corrosion inhibition mechanism. In order to better interpret this process, we propose a magnesium corrosion evaluation in geopolymers and in model alkaline solutions, which simulate the pore solution of these materials after the hydration process.

Material and methods

This work is divided in two parts focusing on the study of magnesium corrosion in the presence of sodium fluoride. The first part consists in verifying Mg-0.5%Zr corrosion when immobilized in Na-geopolymers containing different concentrations of NaF. The second part was performed in model alkaline solutions with concentrations of fluoride equivalent to those found in pore solutions of geopolymers after the hydration process. In both cases, the purpose is to verify the impact of the fluoride concentration on the morphology and nature of the corrosion products and how this reflects on magnesium corrosion rates.

Materials

a) Electrodes and electrochemical system

The same system composed of three electrodes was used in the study of magnesium corrosion in the geopolymer matrices and in the alkaline solutions. The measurements were performed twice for each condition to test their repeatability. The Mg-0.5%Zr alloy samples were provided by Neyco®, whose composition is Mg = 99.95wt.%, Zr = 0.5wt.% (impurities (ppm): Al < 10, As < 20, Co < 10, Cr = 22, Cu = 2, Fe = 9, Mn = 11, Sb < 10, Si < 10, Zn = 31, Cl = 10). They have a cylindrical shape with a diameter of 15 mm and a height of 15 mm, with a total surface area of 10.6 cm^2. The cylinders were polished under ethanol (SiC paper grade 320-1200) and fixed on a threaded steel rod. An electrical insulation was provided by a heat-shrinkable sleeve and by Araldite ®. These Mg-Zr electrodes were stored under vacuum before utilization.

Two configurations were used: in the first one, the alloy was immobilized for 28 days in different geopolymer mortars before coming into contact with NaOH solutions with a pH 12.5 (± 0.1); in the second one, they were placed directly in contact with 400 mL of alkaline solutions containing NaF, with a pH 12.5 (± 0.1). The counter electrode is a titanium grid. All potentials are given with respect to the Hg/HgO (KOH 0.1 $mol.L^{-1}$) reference electrode (-0.076 V *vs.* SCE at 25°C) and all electrodes were connected to a Gamry REF600 potentiostat (Figure 1).

For each condition, non-polarized samples were reserved for the subsequent characterization of the corrosion products naturally formed on the magnesium surface.

b) Geopolymer mortars

The geopolymer mortars were made by mixing metakaolin powder (Argical M1000, AGS Mineraux, whose composition (% wt.) is SiO_2 = 54.4, Al_2O_3 = 38.4, Fe_2O_3 = 1.27, K_2O = 0.62 and TiO_2 = 1.6) and sand (VX800LS, Fulchiron) with an activation solution (AS). This solution was prepared 24h before by dissolving sodium hydroxide (>98%, Prolabo) and sodium fluoride (>98%, Merck) in amorphous silica solution (Betol 39T, Woellner) in ultra-pure milliQ water (18.2 MΩ.cm). All mortars have an initial activation solution to metakaolin ratio (AS/MK) of 0.5 and a sand to metakaolin ratio (S/MK) equal to 2. Table 1 gives the necessary proportions for manufacturing all mortars. Five formulations were chosen in order to verify the impact of the fluoride concentration on corrosion. The concentrations 0.05, 0.36, 0.80 and 1.25 mol.L^{-1} of NaF correspond to those initially added to the activation solution of the geopolymer.

These electrodes were stored for 28 days under 98% relative humidity before utilization, considering that this is the time needed for it to reach its final structure [14].

c) Electrolytes

The solutions were prepared using ultrapure milliQ water at 18.2 MΩ.cm. All pH values were adjusted to 12.5 and the measurement was made using a pHM240 MeterLab pH meter with a combined pH electrode (PHC2011-8), both from Radiometer Analytical. To ensure that the probe is working properly, a calibration of the system was done using four standard solutions at pH 7.01, pH 10.10, pH 12.00 and pH 12.45. The redox potential (Eh) was measured using a MeterLab pHM201 device with a HI3131 internal platinum reference electrode from HANNA Instruments. The proper functioning of the electrode was verified by performing redox potential measurements in standard solutions at 250, 465 and 650 mV. Table 2 contains the chemical composition, the pH and the redox potential of each electrolyte.

The four NaF concentrations selected in this part were related with geopolymer mortars and consider that only 60% of the fluoride initially incorporated in their formulation is present in their pore solution after 28 days of cure [15].

Electrochemical measurements

An open circuit potential measurement was initially performed during 24 hours for embedded samples or 72 hours for non-embedded electrodes, followed by polarization measurements. A potentiodynamic polarization scan was performed for the non-embedded electrodes starting from -0.04V to 2V *vs.* E_{OCP} with a scan rate of 0.1 mV.s^{-1}.

Polarization curves were used to characterize the electrochemical behaviour of the electrode/electrolyte system, which required the system to achieve a permanent regime. In the case of the embedded samples, the time to reach a quasi-stationary state can be long, so it was decided to apply the protocol developed by Laurens *et al.* [16], obtaining a steady-state polarization response of the system by sequential potentiostatic polarization scans. A polarization of ± 0.45V *vs.* E_{OCP} was performed with 18 potential steps of 360 seconds each. The measured potential values (E_{meas}) were corrected of the ohmic loss by the Eq. 1, using the electrical resistance of the mortar (R) and the current (I).

$$\Delta E = \Delta E_{meas} - R \cdot I \qquad \text{Eq. 1}$$

From the current densities obtained by the Tafel extrapolation method of the polarization curves, it was possible to calculate the corrosion rates through Faraday's law, assuming that the dissolution was uniform and considering that two electrons were exchanged in the corrosion process. The application of Tafel extrapolation method is justified in the present

case, since the system presents only one time constant as evidenced by impedance diagrams in previous studies [17], very different from other systems cited in the literature [18,19]. These assumptions were simplified in order to estimate the order of magnitude of the corrosion rates over a year ($\mu m.year^{-1}$), defined by Eq. 2:

$$v_{corr} = 3.15\times10^{11} \cdot \frac{i_{corr} \cdot M}{z \cdot \rho \cdot F} \quad \text{Eq. 2}$$

with i_{corr} the corrosion current density ($A.cm^{-2}$), M the molar mass of the metal ($24.305 g.mol^{-1}$), F the Faraday's constant ($96485 C.mol^{-1}$), z the number of electrons exchanged during the oxidation reaction (z = 2), ρ the specific mass of the metal ($1.74 g.cm^{-3}$) and 3.15×10^{11} a unit conversion factor ($cm.s^{-1}$ to $\mu m.year^{-1}$).

The Eq. 3 evaluated the inhibition efficiency (IE) of the NaF in the uniform corrosion process for the non-embedded samples, where v_{corr} and v^0_{corr} are respectively the corrosion current densities with and without NaF [20].

$$IE\ (\%) = 100 \cdot \frac{v^0_{corr} - v_{corr}}{v^0_{corr}} \quad \text{Eq. 3}$$

Characterization of the corrosion products

The electrodes were characterized with a Scanning Electron Microscopy (SEM), a ZEISS EVO MA15 with a Bruker Quantax Energy Dispersion Spectrometer (EDS). For the embedded electrodes, the cross section Mg-Zr/geopolymer was characterized after 28 days of immobilization in each formulation of geopolymer. The protocol before the analysis involved polishing them under ethanol to #1200 grit (SiC paper) using an automatic Struers Tegramin-30 polisher and finished with 9 µm and 3 µm diamond suspensions an finally the MD Chem polishing cloth, lubricated with a colloidal silica solution. All the samples were metallized with carbon before SEM-EDS analysis.

Additionally to the SEM-EDS analysis, an extra characterization via X-Ray diffraction was performed for the non-embedded electrodes. Both these analysis were done on their surfaces after 28 days in contact with alkaline solutions using a PANalytical X'Pert diffractometer.

Results and Discussion

Corrosion in geopolymers

Before the potentiostatic polarization tests, the magnesium samples were immobilized for 28 days in the geopolymers, undergoing an initial corrosion process. The Figure 2 shows the interface of the Mg-Zr/geopolymer for the five mortar mixes (cracks observed in the geopolymer matrix are a consequence of the sample preparation). The sample without NaF was significantly more corroded, with corrosion products thicknesses reaching up to 150µm.

In the absence of fluorides in alkaline pH levels, thermodynamics suggests the formation of a Brucite ($Mg(OH)_2$) layer [21], confirmed by SEM-EDS characterization in Figure 3. This layer is often listed as porous [22,23], allowing the dissolution and migration of the magnesium towards the interior of the geopolymer, penetrating up to 200µm and creating a transformed medium (mixed zone containing elements coming from the corrosion products and from the geopolymer mortar).

The addition of NaF, even in small concentrations, drastically reduces the corrosion at the Mg-Zr/geopolymer interface, reinforcing its inhibitor character. However, the corrosion rates

calculated from the polarization curves (Figure 4 and Table 3) show surprisingly also a low corrosion rate for the sample without NaF.

The polarization curves performed after 28 days give instantaneous corrosion rates. The SEM-EDS analysis shows the corrosion background of the samples since their fabrication. The Mg-Zr alloy may have undergone strong corrosion process in the absence of NaF in the first few days, which then decreased sharply until 28 days, explaining the subsequent low corrosion rate measured.

The low anodic current densities presented by the sample without NaF may also be related to the fact that the initial layer formed during the first 28 days acts as a physical barrier during polarization, adding an extra resistance to the current flow [24]. However, the estimated corrosion rates in the presence of NaF are consistent with the thicknesses measured by SEM (Figure 2).

The chemical composition of the Mg-Zr/GP 0.05 NaF interface shown in Figure 5(a) revealed no peak concentration of fluoride in the presence of 0.05 mol.L^{-1} of NaF in the activating solution. However, the difference in the corrosion levels compared to the case without NaF implies an inhibiting effect by these ions. Small concentrations of fluoride induce the formation of a magnesium fluoride layer (MgF_2), often in the form of a layer of nanometric thickness [25,26], making it difficult to identify with EDS analysis. The same layer may be present in the second case (Figure 5(b)) where only 5 at.% of fluoride was detected at the interface. This film may nonetheless undergo morphology transformations depending on the experimental conditions [27,28], influencing the resulting corrosion rates.

Concentrations of fluoride below 0.30 mol.L^{-1} [5] and above 1 mol.L^{-1} [3] in solution, have a beneficial effect on the inhibition corrosion process of Mg alloys due to a protection provided by the MgF_2 and $NaMgF_3$ films respectively formed on the magnesium surface. In the case of Mg-Zr corrosion in geopolymer, this process seems to be similar for the concentrations below 0.36 mol.L^{-1} and above 1.25 mol.L^{-1} of NaF in the AS. The inhibition process seems to be more effective in these concentrations than for the 0.80 mol.L^{-1} of NaF in the AS, which is the most corroded sample, presenting 15-12 at.% of fluoride at the Mg-Zr/geopolymer interface (Figure 6(a)) and not corresponding to any of the fluoride compounds mentioned above. In the case of 1.25 mol.L^{-1} of NaF in the AS (Figure 6(b)), 60-50 at.% of fluoride was found and the atomic ratio [Mg]/[F] corresponds to the Neighborite ($NaMgF_3$), which has an inhibitor character [4,7].

In both cases, these layers correspond only to 15% of the characterized interface. The other 85% presented a composition similar to that found in the GP 0.36 NaF. Figure 7 shows the corrosion products distribution in the sample with 1.25 mol.L^{-1} of NaF in the AS.

The difference between the compositions of the films formed on the surface of Mg was linked to the concentration of fluoride ions available at the Mg-Zr/geopolymer interface during the corrosion/inhibition process (Figure 8). In cementitious environments, corrosion at the interfaces does not necessarily develop in the same way. Initially, F^- ions in the vicinity of the corroded areas combine with Mg^{2+} ions to form MgF_2. The increase of F^- and Na^+ ions available for the reaction above a certain concentration (0.36 mol.L^{-1}) may breakdown the protection layer and depassivate the metal [5]. This film can undergo structural or chemical transformations, not necessarily possessing the same protective properties – porous layers of MgF_2 were identified in previous studies, being less effective in controlling corrosion [7, 29].

If the first layer does not prevent the dissolution of magnesium, the Mg^{2+} ions continue to react with the F^- ions present at the interface, generating a concentration gradient and stimulating the migration of more fluoride ions from the geopolymer to the corroded areas.

The layer initially formed by MgF_2 can evolve into $NaMgF_3$ [4,7,26], which also possesses protective properties. Nonetheless, a certain concentration is necessary for this evolution to occur [26], and must be greater or equal to 1.25 mol.L^{-1} for this study. For the GP 0.80 NaF sample, the concentration of fluoride present in the interstitial solution was probably sufficient to modify the initially formed MgF_2 film allowing the dissolution of magnesium, but was not high enough to grant the formation of $NaMgF_3$, thus being less effective in reducing corrosion.

Corrosion in alkaline solutions

The solutions at 0, 0.030, 0.215, 0.475 and 0.735 mol.L^{-1} of NaF corresponds in terms of fluoride concentration to geopolymers GP, GP 0.05 NaF, GP 0.36 NaF, GP 0.80 NaF and GP 1.25 NaF, respectively, after 28 curing days. This correlation is summarized in the Table 4.

Figure 9 contains the polarization curves after 72 hours at OCP. The pH was set at 12.5 using NaOH. Table 5 contains the potential, current density, corrosion rates and inhibition efficiencies for the five conditions.

The results suggest that there is a range of fluorine concentration that is more efficient in reducing magnesium corrosion: less than 0.215 mol.L^{-1} and above 0.475 mol.L^{-1} of NaF. It is important to mention that these results cannot be directly transposed to the study in cementitious medium, although they help in the understanding of certain inhibition mechanisms. The presence of the geopolymer induces lower corrosion rates than in the model alkaline solutions. Furthermore, the solid phase ensures the electroneutrality of the system, providing the ions to the pore solution if the corrosion process consumes them.

The least effective concentration of 0.475 mol.L^{-1} of NaF is related to the formulation GP 0.80 NaF presented above. These results are directly related to the morphology and chemical composition of the layer formed on the magnesium surface (Figures 10 and 11).

The X-ray analysis allowed only the identification of the products formed in the absence and presence of 0.735 mol.L^{-1} of NaF – Brucite and Neighborite respectively. The difficulty of identifying the layers formed for the others NaF concentrations may be related to their thickness. However, their surface morphology and chemical composition were different, as shown in Figure 11.

For a NaF concentration of 0.030 mol.L^{-1}, an atomic fluoride concentration similar to the previous case of GP 0.36 NaF was found, inferring that the same MgF_2 layer was formed. In the case of the 0.735 NaF sample, only $NaMgF_3$ was detected on the magnesium surface. The layers identified in these two cases were the most effective to reduce corrosion. Figure 12 shows a schematic representation of the change in morphology and chemical composition of the films formed on the magnesium surface and its impact on the corrosion rates.

The increase in fluoride concentration to 0.215 mol.L^{-1} modified the morphology of the first film, being less efficient to protect magnesium, achieving the maximum corrosion at 0.475 mol.L^{-1}. The percentage of fluorine detected in the corrosion layer for these two cases is similar to that found in the geopolymer containing 0.80 mol.L^{-1} of NaF – approximately 15 at.%. Moving to intermediate concentrations of NaF induces the change of the MgF_2 layer initially formed, compromising magnesium protection. The rupture in the passive layer seems to be greater in the presence of 0.475 mol.L^{-1} of fluoride than in 0.215 mol.L^{-1}. In both cases, the F^- concentration is not high enough to cause the evolution in $NaMgF_3$, as in the presence of 0.735 mol.L^{-1} of NaF, compromising the inhibition mechanism.

The films were homogenously distributed over the surfaces because, in model alkaline solutions, fluoride ions diffuse more easily than in cementitious media. However, the formation mechanism of these products at the interface and their inhibition effectiveness seem to follow the same trend in both studies. Small and high concentrations of F^- were equally beneficial, however the addition of an excess NaF ensures the formation of $NaMgF_3$ (if corrosion levels increase in certain areas of the material).

Conclusion

In all the cases presented here, it was clear that the fluoride present in pore solutions of geopolymers, even in small concentrations, was efficient in reducing the corrosion at the Mg-Zr/geopolymer interface. The formulations with 0.05, 0.36 and 1.25 $mol.L^{-1}$ of NaF in the activation solution of the geopolymers, were however the most effective in inhibiting corrosion. There is a probable formation of MgF_2 in all cases and this film can evolve into $NaMgF_3$ for the highest fluoride concentration.

It was expected that approximately 0.475 $mol.L^{-1}$ of F^- were present in the pore solution of GP 0.80 NaF formulation after 28 days of hydration. The results obtained whether in solution or geopolymer for these two cases render them less adequate to reduce corrosion. Concentrations below 0.215 $mol.L^{-1}$ and above 0.475 $mol.L^{-1}$ in solution or in pore solution are more recommended. In all cases, the results are directly related to the morphology and the composition of the layers formed in the Mg-Zr surface.

Corrosion rates in cementitious media were lower than those measured in alkaline solutions. Despite the convenience of solutions experiments, they should be used only as a complement to these performed on the mortar, without ever replacing it. The study enabled the observation of structural changes of the fluoride films formed on the magnesium surface induced by the variation of the NaF concentration. However, these films are uniformly distributed, differently from the embedded electrodes. In this case, the morphology and chemical composition of the products formed at the Mg-Zr/geopolymer interface depends on the concentration of fluoride available for the reaction and its migration through the cementitious matrix, as well as on the evolution of the corrosion process.

Acknowledgments

Financial support from the CEA (Commissariat à l'Energie Atomique et aux Energies Alternatives) and from ORANO.

Data availability

The raw/processed data required to reproduce these findings cannot be shared at this time as the data also forms part of an ongoing study.

References

[1] D. Lambertin, F. Frizon, F. Bart, Mg-Zr alloy behavior in basic solutions and immobilization in Portland cement and Na-geopolymer with sodium fluoride inhibitor, Surf. Coat. Technol. 206 (2012) 4567–4573. https://doi.org/10.1016/j.surfcoat.2012.05.008.

[2] A. Rooses, D. Lambertin, D. Chartier, F. Frizon, Galvanic corrosion of Mg–Zr fuel cladding and steel immobilized in Portland cement and geopolymer at early ages, J. Nucl. Mater. 435 (2013) 137–140. https://doi.org/10.1016/j.jnucmat.2012.12.030.

[3] E. Gulbrandsen, J. Taftø, A. Olsen, The passive behaviour of Mg in alkaline fluoride solutions. Electrochemical and electron microscopical investigations, Corros. Sci. 34 (1993) 1423–1440. https://doi.org/10.1016/0010-938X(93)90238-C.

[4] F. El-Taib Heakal, N.S. Tantawy, O.S. Shehata, Impact of chloride and fluoride additions on surface reactivity and passivity of AM60 magnesium alloy in buffer solution, Corros. Sci. 64 (2012) 153–163. https://doi.org/10.1016/j.corsci.2012.07.011.

[5] F. El-Taib Heakal, A.M. Fekry, M.Z. Fatayerji, Influence of halides on the dissolution and passivation behavior of AZ91D magnesium alloy in aqueous solutions, Electrochim. Acta. 54 (2009) 1545–1557. https://doi.org/10.1016/j.electacta.2008.09.055.

[6] F.B. Mainier, A.A.M. Figueiredo, A.E.R. de Freitas, A.A.M. de A. Junior, The Use of Sodium Silicate as a Corrosion Inhibitor in a Saline Drilling Fluid: A Nonaggressive Option to the Environment, J. Environ. Prot. 07 (2016) 2025–2035. https://doi.org/10.4236/jep.2016.713157.

[7] A.A. Zuleta, E. Correa, J.G. Castaño, F. Echeverría, A. Baron-Wiecheć, P. Skeldon, G.E. Thompson, Study of the formation of alkaline electroless Ni-P coating on magnesium and AZ31B magnesium alloy, Surf. Coat. Technol. 321 (2017) 309–320. https://doi.org/10.1016/j.surfcoat.2017.04.059.

[8] Y. Lv, D. Tang, D. Cao, G. Wang, M. Zhang, J. Feng, The effect of NaF on the electrochemical behavior of the Mg–11Li–3.5Al–1Zn–1Sn–1Ce–0.1Mn electrode in NaCl solution, RSC Adv. 5 (2015) 46423–46429. https://doi.org/10.1039/C5RA05512A.

[9] J. Xu, Q. Yang, M.S. Javed, Y. Gong, M.K. Aslam, C. Chen, The effects of NaF concentration on electrochemical and corrosion behavior of AZ31B magnesium alloy in a composite electrolyte, RSC Adv. 7 (2017) 5880–5887. https://doi.org/10.1039/C6RA27263K.

[10] Z.P. Yao, X.R. Liu, L.L. Li, S.F. Qi, Z.H. Jiang, Effects of Sodium Fluoride on Structure and Corrosion Resistance of Plasma Electrolytic Oxidation Ceramic Coatings on Magnesium Alloys, Corrosion. 66 (2010) 085002-085002–6. https://doi.org/10.5006/1.3479952.

[11] S. Chakri, P. David, I. Frateur, A. Galtayries, P. Marcus, E. Sutter, B. Tribollet, V. Vivier, S. Zanna, Effet de la composition chimique de la solution interstitielle de bétons jeunes sur la passivation d'un acier doux, Matér. Tech. 103 (2015) 209. https://doi.org/10.1051/mattech/2015016.

[12] T. Yonezawa, V. Ashworth, R.P.M. Procter, Pore Solution Composition and Chloride Effects on the Corrosion of Steel in Concrete, Corrosion. 44 (1988) 489–499. https://doi.org/10.5006/1.3583967.

[13] J. Williamson, O.B. Isgor, The effect of simulated concrete pore solution composition and chlorides on the electronic properties of passive films on carbon steel rebar, Corros. Sci. 106 (2016) 82–95. https://doi.org/10.1016/j.corsci.2016.01.027.

[14] P. Rovnaník, Effect of curing temperature on the development of hard structure of metakaolin-based geopolymer, Constr. Build. Mater. 24 (2010) 1176–1183. https://doi.org/10.1016/j.conbuildmat.2009.12.023.

[15] B. E. Torres-Bautista, J. Agullo, B. Muzeau, C. Bataillon, Study of general and galvanic corrosion of Mg alloys in Na-geopolymer / NaF and its synthetic pore solution, The European Corrosion Congress - Eurocorr (2015).

[16] S. Laurens, P. Hénocq, N. Rouleau, F. Deby, E. Samson, J. Marchand, B. Bissonnette, Steady-state polarization response of chloride-induced macrocell corrosion systems in

steel reinforced concrete — numerical and experimental investigations, Cem. Concr. Res. 79 (2016) 272–290. https://doi.org/10.1016/j.cemconres.2015.09.021.

[17] B. E. Torres-Bautista, J. Agullo, B. Muzeau, C. Bataillon, Study of the galvanic corrosion behaviour of Mg alloys in synthetic Na-geopolymer/NaF pore solution, proceeding EUROCORR 2016.

[18] S. Leleu, B. Rives, N. Causse, N. Pébère, Corrosion rate determination of rare-earth Mg alloys in a Na_2SO_4 solution by electrochemical measurements and inductive coupled plasma-optical emission spectroscopy, Journal of Magnesium and Alloys 7 (2019) 47-57. https://doi.org/10.1016/j.jma.2018.12.002.

[19] G. Baril, G. Galicia, C. Deslouis, N. Pébère, B. Tribollet, V Vivier, An Impedance Investigation of the Mechanism of Pure Magnesium Corrosion in Sodium Sulfate Solutions, J. Electrochem. Soc., 154 (2007) C108–C113. https://doi.org/10.1149/1.2401056.

[20] A. Elhebshi, M. S. El-Deab, A. El nemr, I. Ashour, Corrosion Inhibition Efficiency of Cysteine-Metal ions Blends on Low Carbon Steel in Chloride-Containing Acidic Media, Int. J. Electrochem. Soc. 14 (2019) 3897 – 3915. https://doi.org/10.20964/2019.03.51.

[21] M. Pourbaix, Atlas of electrochemical equilibria in aqueous solutions, National Association of Corrosion Engineers, (1974).

[22] G.-L. Song, 1 - Corrosion electrochemistry of magnesium (Mg) and its alloys, Corros. Magnes. Alloys, Woodhead Publishing, (2011) 3–65. https://doi.org/10.1533/9780857091413.1.3.

[23] D.A. Vermilyea, C.F. Kirk, Studies of Inhibition of Magnesium Corrosion, J. Electrochem. Soc. 116 (1969) 1487–1492. https://doi.org/10.1149/1.2411579.

[24] S. Li, Z. Chen, F. Wang, B. Cui, L. Tan, F. Bobaru, Analysis of Corrosion-Induced Diffusion Layer in ZK60A Magnesium Alloy, J. Electrochem. Soc. 163 (2016) C784–C790. https://doi.org/10.1149/2.1001613jes.

[25] W.P. Hsu, Q. Zhong, E. Matijević, The Formation of Uniform Colloidal Particles of Magnesium Fluoride and Sodium Magnesium Fluoride, J. Colloid Interface Sci. 181 (1996) 142–148. https://doi.org/10.1006/jcis.1996.0365.

[26] I. Sevonkaev, D.V. Goia, E. Matijević, Formation and structure of cubic particles of sodium magnesium fluoride (neighborite), J. Colloid Interface Sci. 317 (2008) 130–136. https://doi.org/10.1016/j.jcis.2007.09.036.

[27] A.B.D. Nandiyanto, F. Iskandar, T. Ogi, K. Okuyama, Nanometer to Submicrometer Magnesium Fluoride Particles with Controllable Morphology, Langmuir. 26 (2010) 12260–12266. https://doi.org/10.1021/la101194w.

[28] I. Sevonkaev, E. Matijević, Formation of Magnesium Fluoride Particles of Different Morphologies, Langmuir. 25 (2009) 10534–10539. https://doi.org/10.1021/la901307t.

[29] Z. Zhang, G. Yu, Y. Ouyang, X. He, B. Hu, J. Zhang, Z. Wu, Studies on influence of zinc immersion and fluoride on nickel electroplating on magnesium alloy AZ91D, Appl. Surf. Sci. 255 (2009) 7773–7779. https://doi.org/10.1016/j.apsusc.2009.04.169.

Figure Captions

Figure 1: Electrodes used for electrochemical data acquisitions: (a) geopolymer embedded and (b) non-embedded electrodes.

Figure 2: SEM micrography of Mg-Zr/geopolymer interface after 28 days of hydration.

Figure 3: Chemical analysis by SEM-EDS of Mg-Zr/geopolymer interface without NaF, with CP = corrosion products and TM = transformed medium.

Figure 4: Polarization curves of magnesium in different geopolymer mortars.

Figure 5: SEM-EDS analysis of Mg-Zr/geopolymer interface with (a) 0.05 mol.L^{-1} and (b) 0.36 mol.L^{-1} of NaF in the activating solution.

Figure 6: Mg-Zr/geopolymer interface with (a) 0.80 mol.L^{-1} and (b) 1.25 mol.L^{-1} of NaF in the AS.

Figure 7: The non-uniform distribution of corrosion products at the Mg-Zr/ GP 1.25 NaF interface.

Figure 8: Schematic representation of the corrosion process in geopolymer in the presence of fluoride, with TM = transformed medium.

Figure 9: Polarization curves of magnesium in model alkaline solutions.

Figure 10: Comparison between X-ray diffraction patterns obtained after 28 days of immersion in different alkaline solutions.

Figure 11: SEM-EDS analysis of magnesium corrosion products formed in alkaline solutions containing NaF.

Figure 12: Schematic representation of the corrosion process in the presence of fluoride.

Tables

Table 1: Chemical composition of activation solutions and mortars (kg.m^{-3}).

Products		Concentration (kg.m^{-3})				
		GP	GP 0.05 NaF	GP 0.36 NaF	GP 0.80 NaF	GP 1.25 NaF
Activation solution (AS)	NaOH	73.35	73.35	73.35	73.35	73.35
	Amorphous silica	579.97	579.97	579.97	579.97	579.97
	NaF	0	0.81	5.85	12.94	20.02
	Water	9.90	9.90	9.90	9.90	9.90
Metakaolin (MK)		450.00	450.00	450.00	450.00	450.00
Sand (S)		900.00	900.00	900.00	900.00	900.00
AS/MK		0.5	0.5	0.5	0.5	0.5
S/MK		2	2	2	2	2

Table 2: Chemical compositions of the model alkaline solutions

Reagents	Concentration (mol.L^{-1})				
	0 NaF	0.030 NaF	0.215 NaF	0.475 NaF	0.735 NaF
NaOH	0.035	0.039	0.047	0.051	0.052
NaF	-----	0.030	0.215	0.475	0.735
pH (± 0,1)	12.5	12.5	12.5	12.5	12.5
Eh (mV)	36	-88	-103	-84	-16

Table 3: E_{corr}, i_{corr} and v_{corr} calculated from the magnesium polarization curves in geopolymer.

	E_{corr} (V *vs.* SCE)	i_{corr} ($A.cm^{-2}$)	v_{corr} ($\mu m.year^{-1}$)
GP	-1.251	$6.46x10^{-9}$	0.15
GP 0.05 NaF	-1.181	$6.95x10^{-9}$	0.16
GP 0.36 NaF	-1.161	$8.51x10^{-9}$	0.19
GP 0.80 NaF	-1.211	$2.85x10^{-8}$	0.65
GP 1.25 NaF	-1.161	$1.23x10^{-8}$	0.28

Table 4: Correlation between geopolymer mortars and alkaline solutions

Geopolymer mortar	Corresponding alkaline solution
GP	0 NaF
GP 0.05 NaF	0.030 NaF
GP 0.36 NaF	0.215 NaF
GP 0.80 NaF	0.475 NaF
GP 1.25 NaF	0.735 NaF

Table 5: E_{corr}, i_{corr}, v_{corr} and IE calculated from the magnesium polarization curves in alkaline solutions.

	E_{corr} (V *vs.* SCE)	i_{corr} ($A.cm^{-2}$)	v_{corr} ($\mu m.year^{-1}$)	IE (%)
0 NaF	-1.091	$8.76x10^{-8}$	2.00	0
0.030 NaF	-0.741	$3.79x10^{-9}$	0.08	96.00
0.215 NaF	-1.311	$4.82x10^{-8}$	1.10	45.00
0.475 NaF	-1.451	$3.94x10^{-7}$	9.01	-350.50
0.735 NaF	-0.911	$1.57x10^{-8}$	0.35	82.50

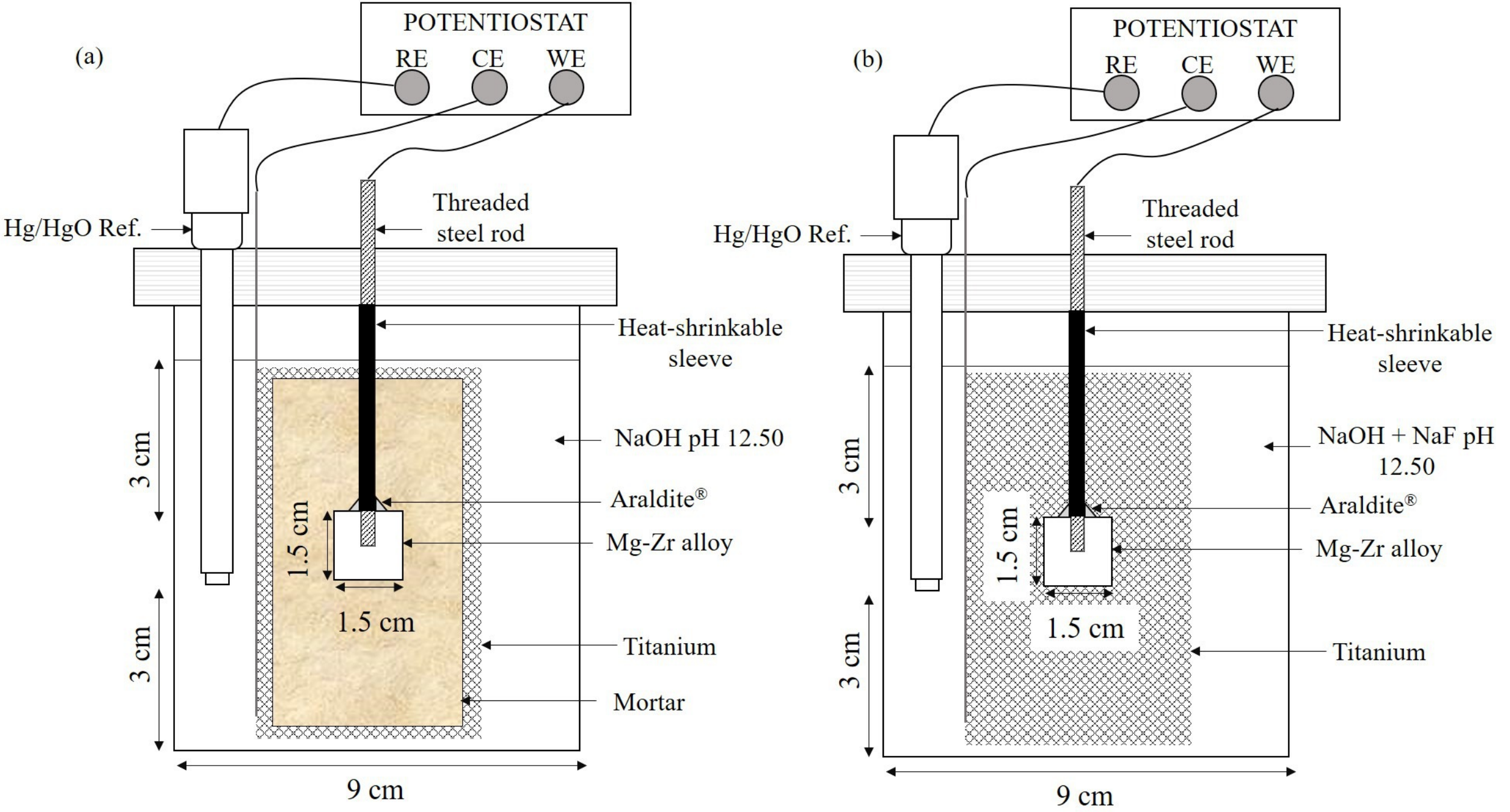
(a)
POTENTIOSTAT
RE
CE
WE
Hg/HgO Ref.
Threaded steel rod
Heat-shrinkable sleeve
NaOH pH 12.50
Araldite®
Mg-Zr alloy
Titanium
Mortar
3 cm
1.5 cm
3 cm
1.5 cm
9 cm
(b)
POTENTIOSTAT
RE
CE
WE
Hg/HgO Ref.
Threaded steel rod
Heat-shrinkable sleeve
NaOH + NaF pH 12.50
Araldite®
Mg-Zr alloy
Titanium
3 cm
1.5 cm
3 cm
1.5 cm
9 cm

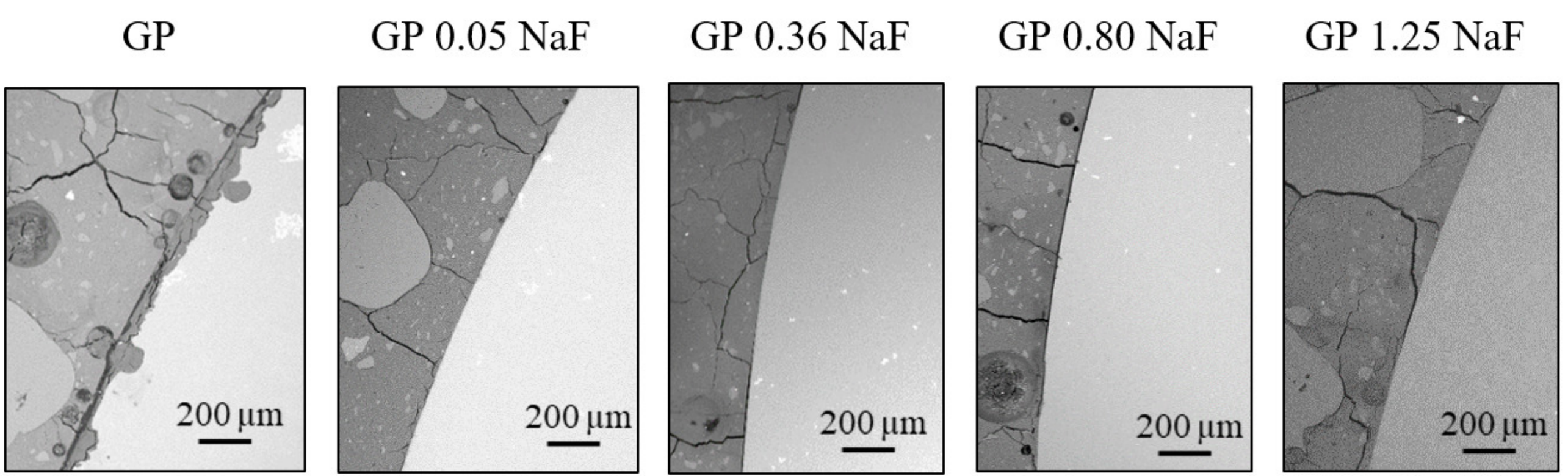
GP
GP 0.05 NaF
GP 0.36 NaF
GP 0.80 NaF
GP 1.25 NaF
200 µm
200 µm
200 µm
200 µm
200 µm

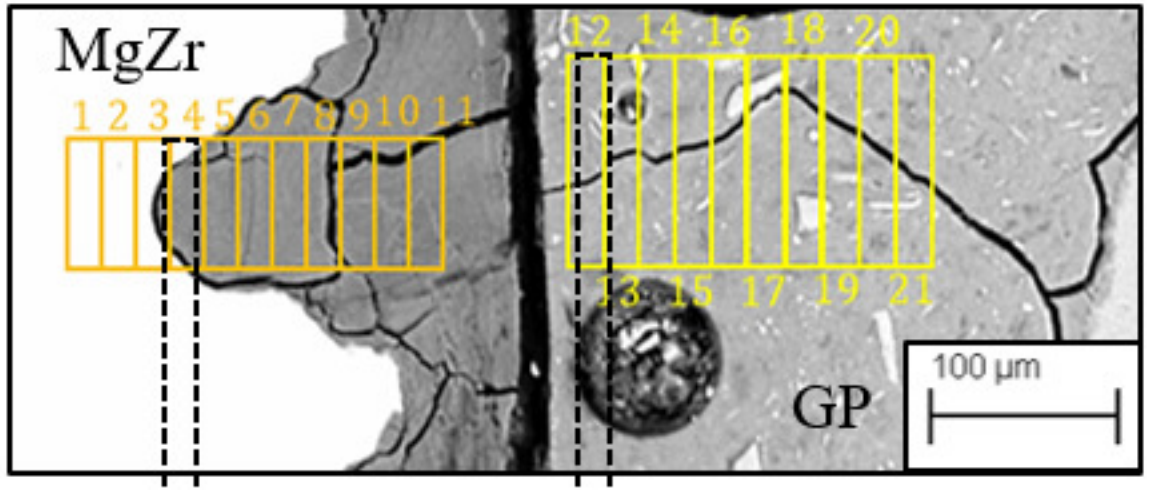
MgZr
1 2 3 4 5 6 7 8 9 10 11
12 14 16 18 20
13 15 17 19 21
GP
100 µm

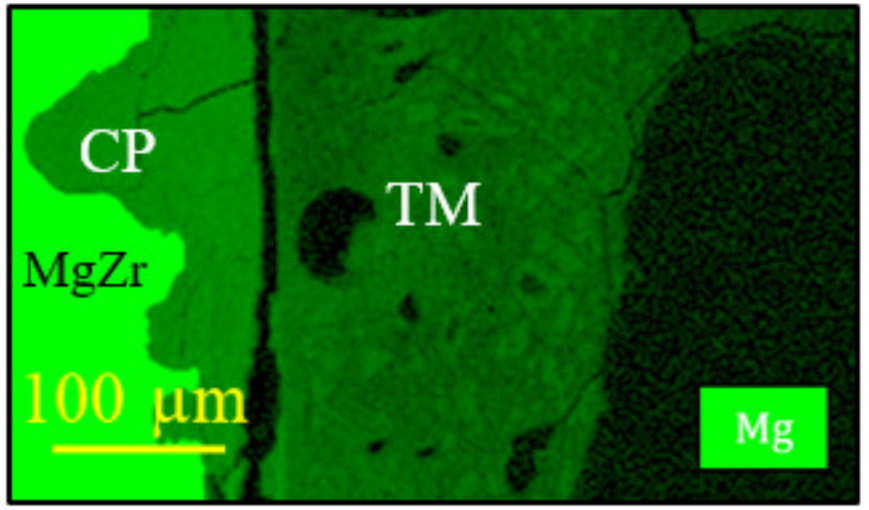
CP
TM
MgZr
100 µm
Mg

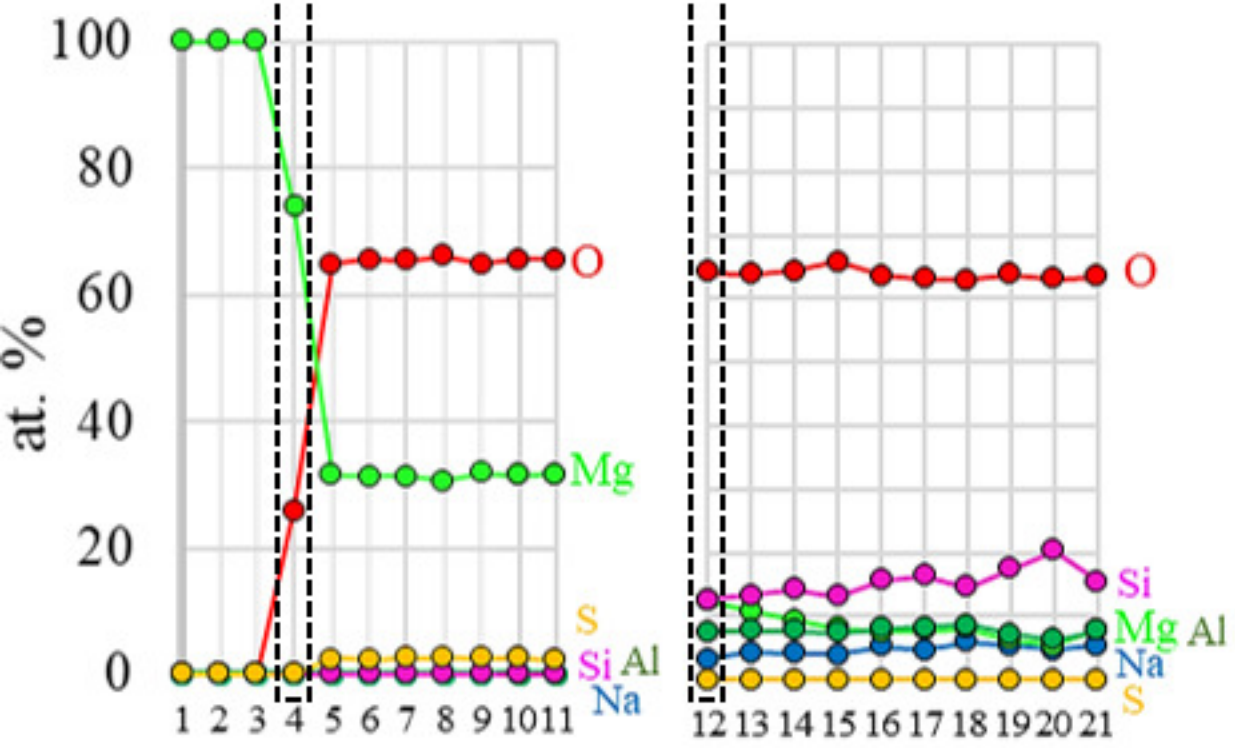
100
80
60
40
20
0
at. %
O
Mg
S
Si Al
Na
1 2 3 4 5 6 7 8 9 10 11
12 13 14 15 16 17 18 19 20 21
O
Si
Mg Al
Na
S

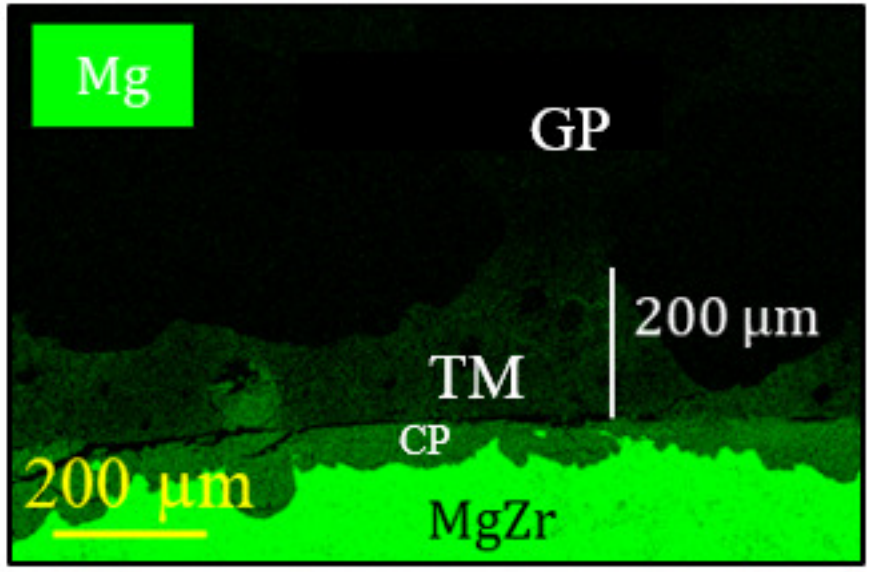
Mg
GP
200 µm
TM
CP
200 µm
MgZr

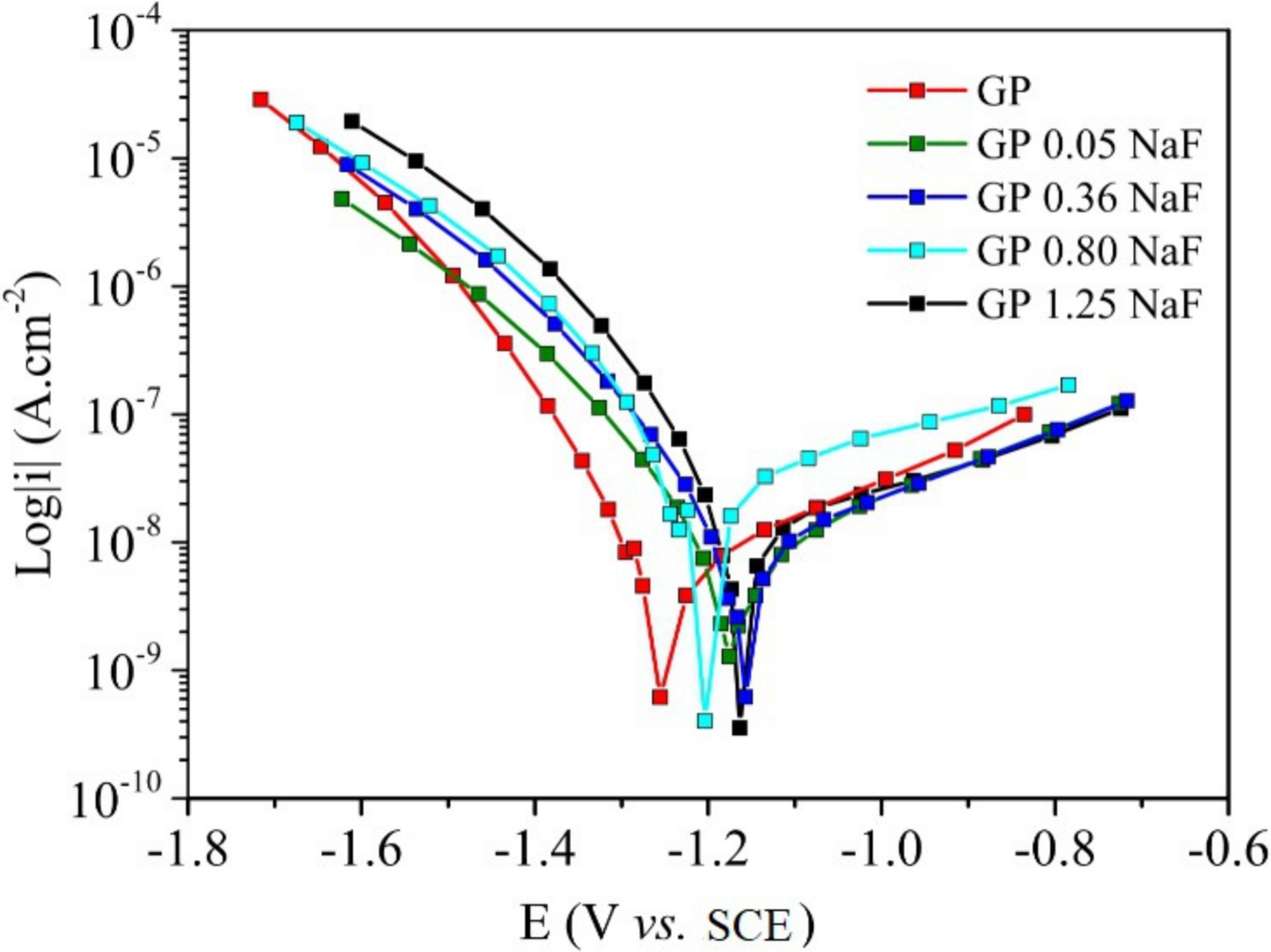
GP
GP 0.05 NaF
GP 0.36 NaF
GP 0.80 NaF
GP 1.25 NaF
Log|i| (A.cm-2)
E (V vs. SCE)
10-4
10-5
10-6
10-7
10-8
10-9
10-10
-1.8
-1.6
-1.4
-1.2
-1.0
-0.8
-0.6

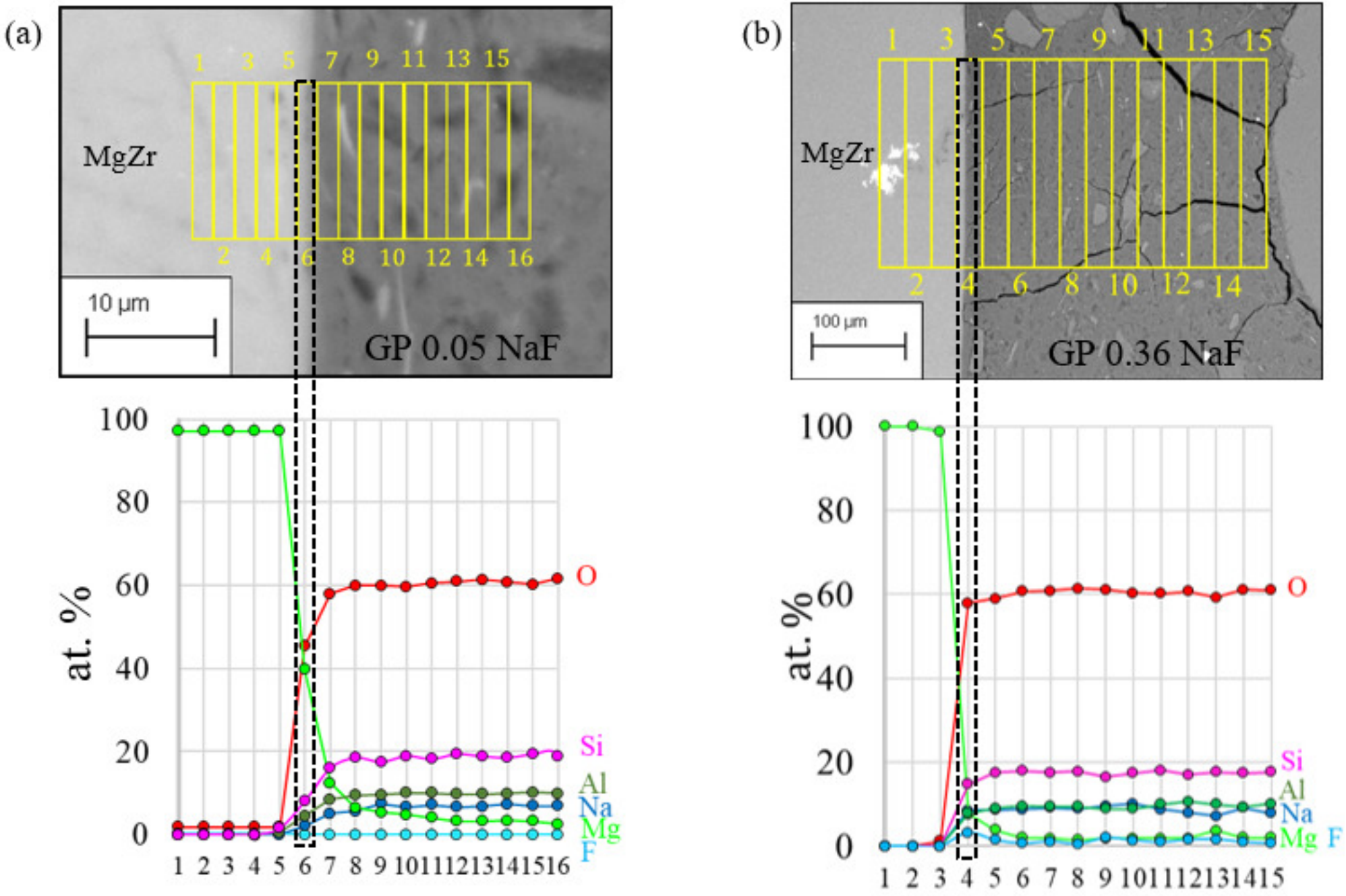
(a)
MgZr
1 3 5 7 9 11 13 15
2 4 6 8 10 12 14 16
10 µm
GP 0.05 NaF
100
80
60
40
20
0
at. %
O
Si
Al
Na
Mg
F
1 2 3 4 5 6 7 8 9 10 11 12 13 14 15 16
(b)
MgZr
1 3 5 7 9 11 13 15
2 4 6 8 10 12 14
100 µm
GP 0.36 NaF
100
80
60
40
20
0
at. %
O
Si
Al
Na
Mg
F
1 2 3 4 5 6 7 8 9 10 11 12 13 14 15

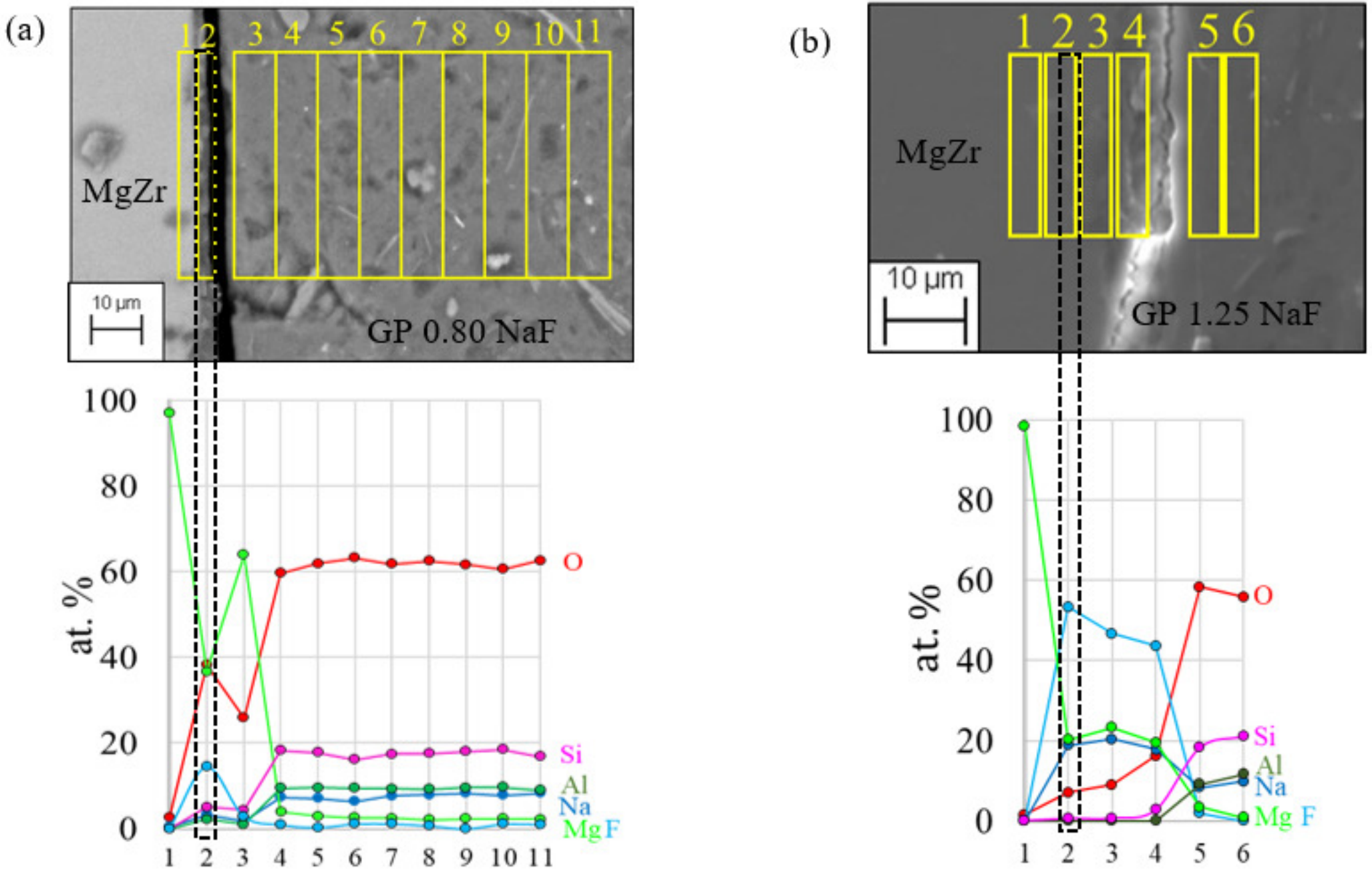
(a)
1 2 3 4 5 6 7 8 9 10 11
MgZr
10 µm
GP 0.80 NaF
100
80
60
40
20
0
at. %
O
Si
Al
Na
Mg F
1 2 3 4 5 6 7 8 9 10 11
(b)
1 2 3 4 5 6
MgZr
10 µm
GP 1.25 NaF
100
80
60
40
20
0
at. %
O
Si
Al
Na
Mg F
1 2 3 4 5 6

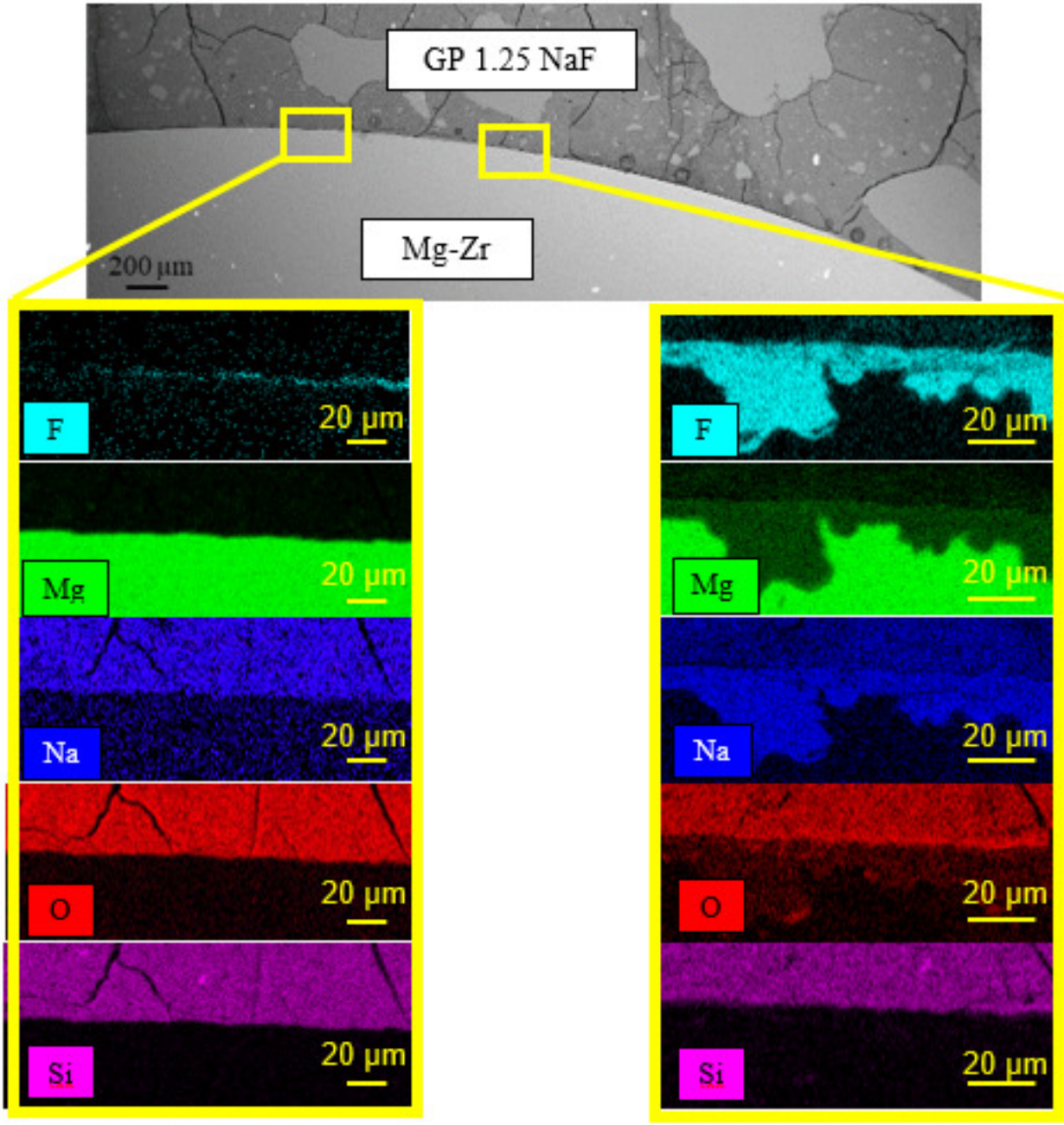
GP 1.25 NaF
Mg-Zr
200 µm
F
20 µm
Mg
20 µm
Na
20 µm
O
20 µm
Si
20 µm
F
20 µm
Mg
20 µm
Na
20 µm
O
20 µm
Si
20 µm

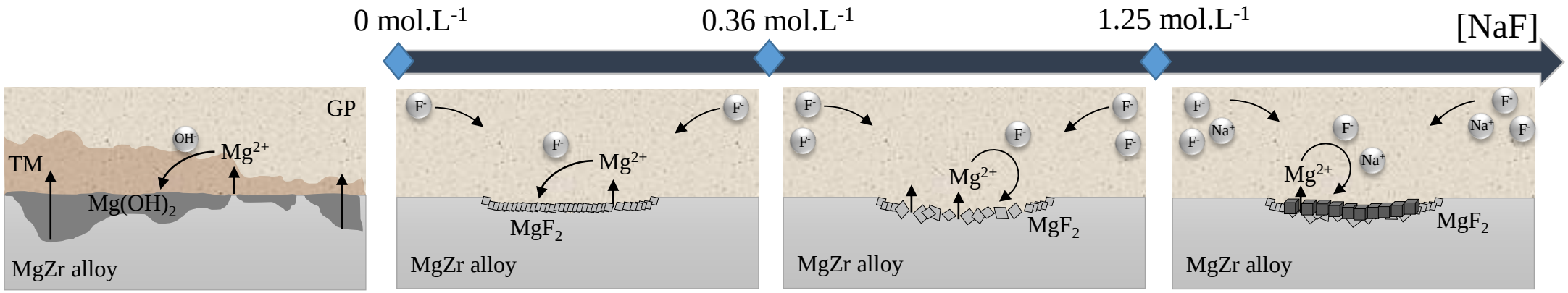

Formation of $Mg(OH)_2$

Formation of MgF_2

Destabilization of MgF_2 layer
and/or
modification of its morphology

Formation of $NaMgF_3$

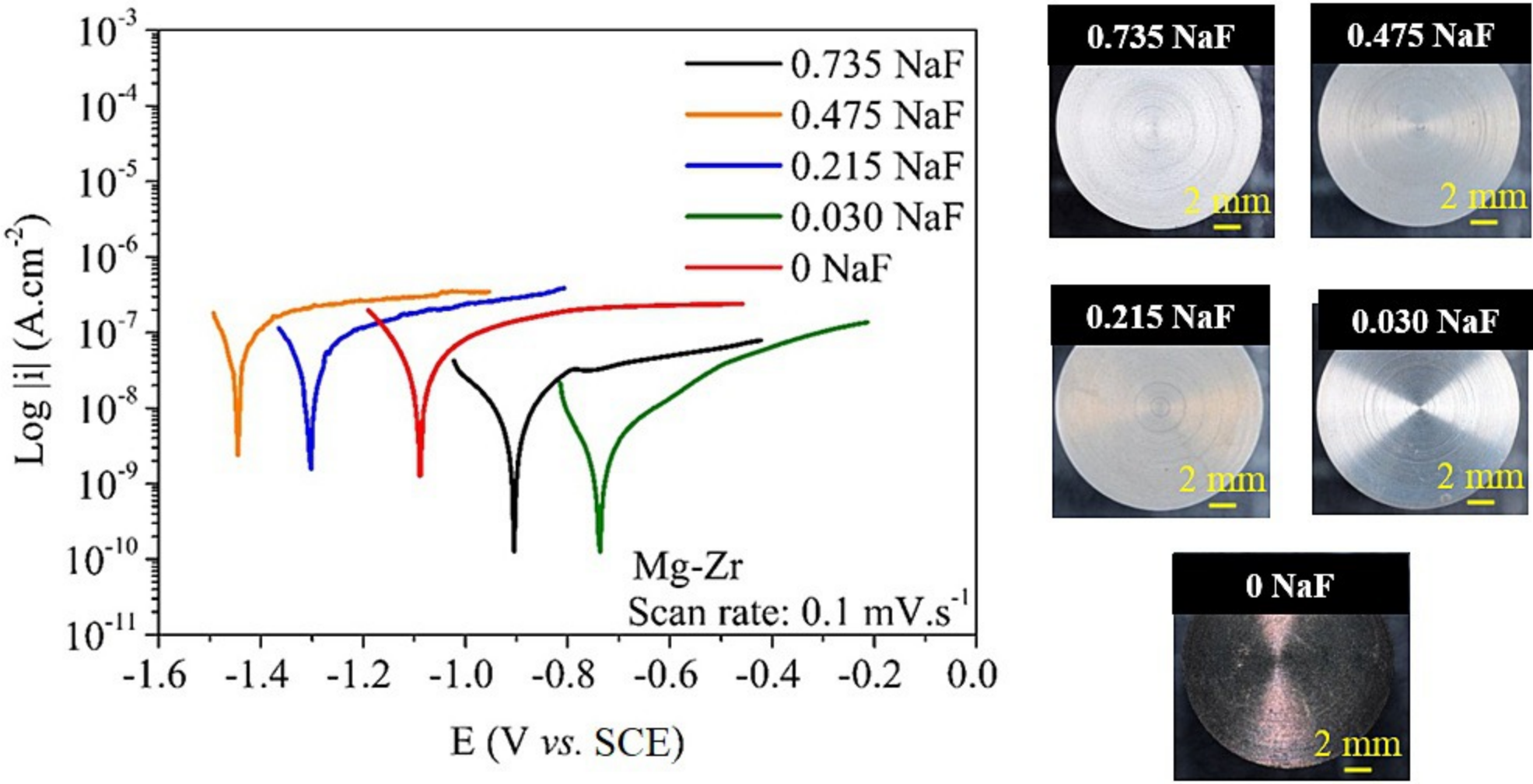
0.735 NaF
0.475 NaF
0.215 NaF
0.030 NaF
0 NaF
Mg-Zr
Scan rate: 0.1 mV.s-1
Log |i| (A.cm-2)
E (V vs. SCE)
10-3
10-4
10-5
10-6
10-7
10-8
10-9
10-10
10-11
-1.6
-1.4
-1.2
-1.0
-0.8
-0.6
-0.4
-0.2
0.0
0.735 NaF
2 mm
0.475 NaF
2 mm
0.215 NaF
2 mm
0.030 NaF
2 mm
0 NaF
2 mm

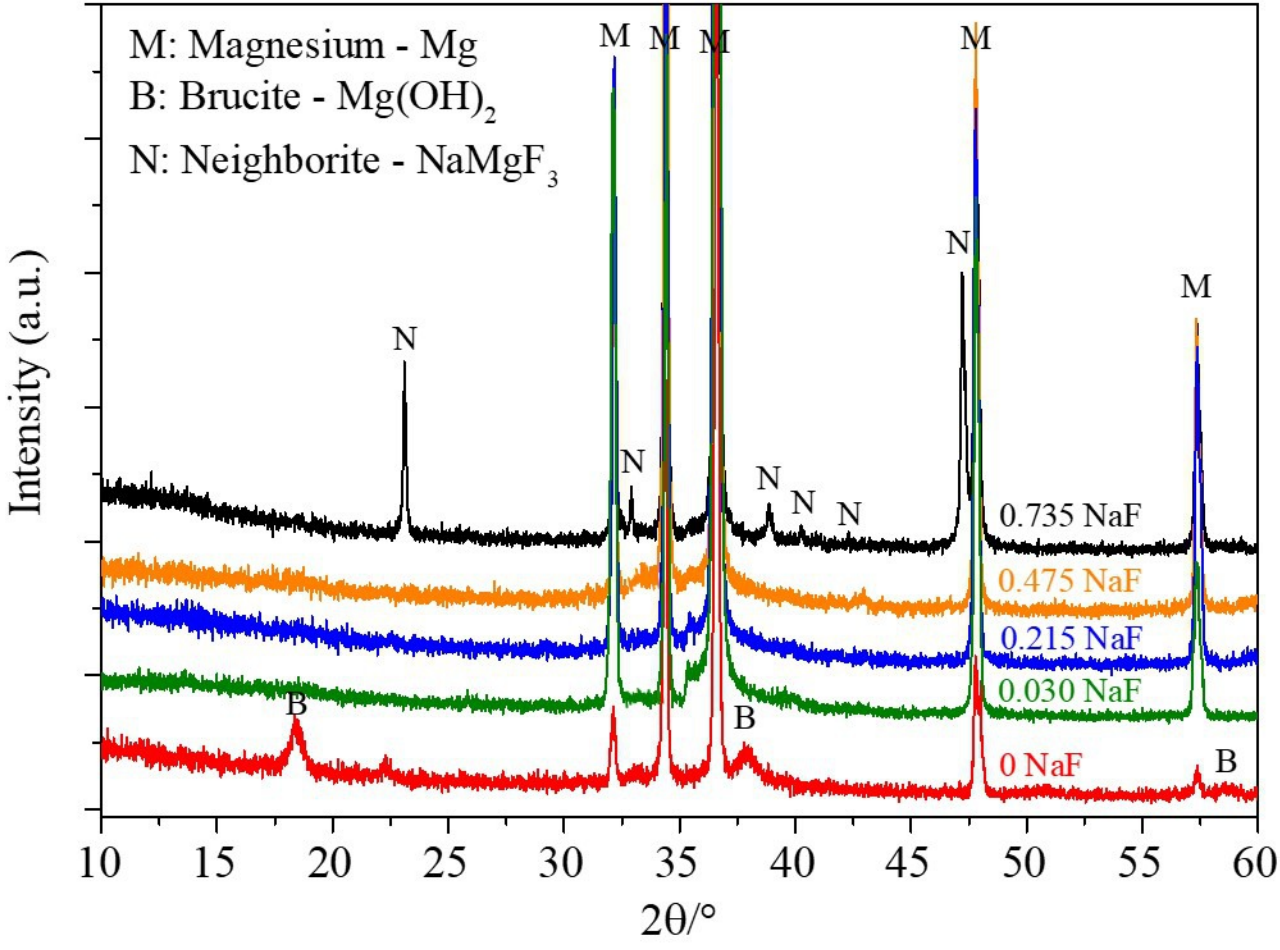
M: Magnesium - Mg
B: Brucite - Mg(OH)2
N: Neighborite - NaMgF3
Intensity (a.u.)
2θ/°
0.735 NaF
0.475 NaF
0.215 NaF
0.030 NaF
0 NaF
M
N
B
10
15
20
25
30
35
40
45
50
55
60

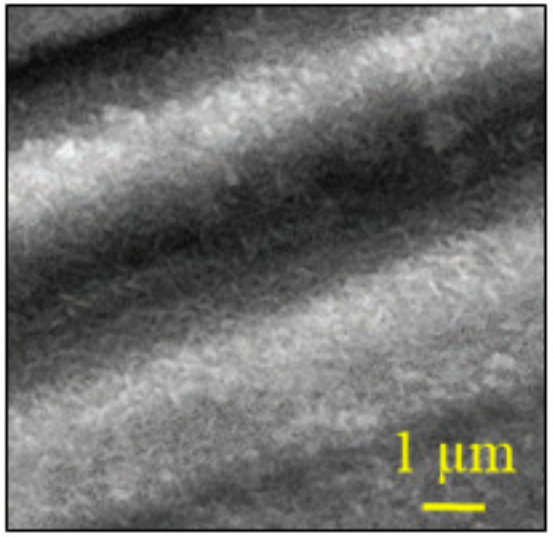

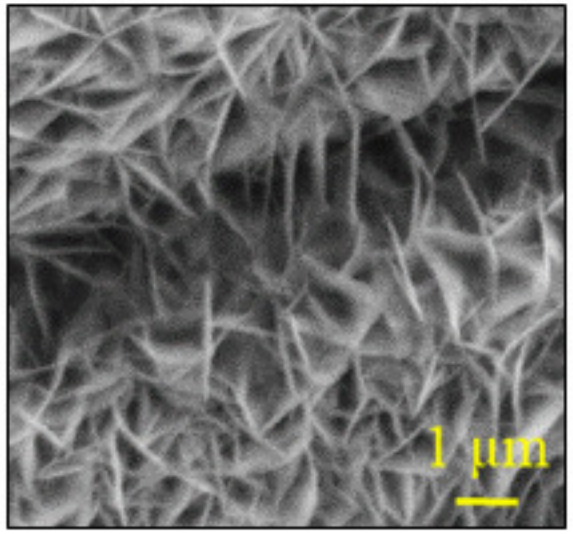

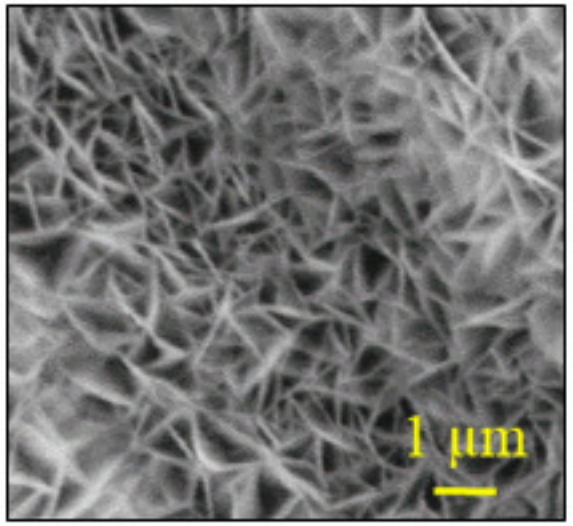

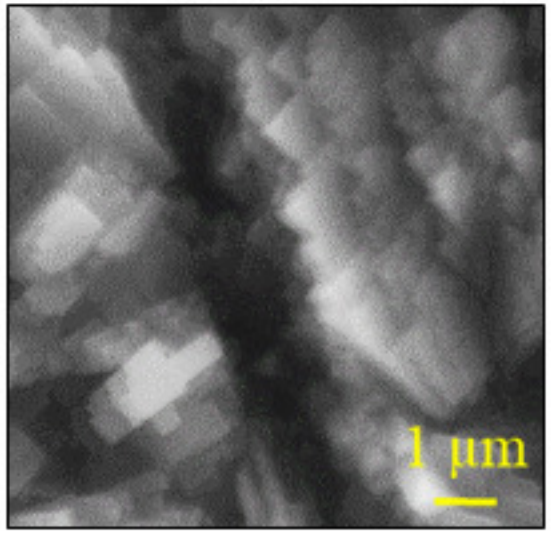

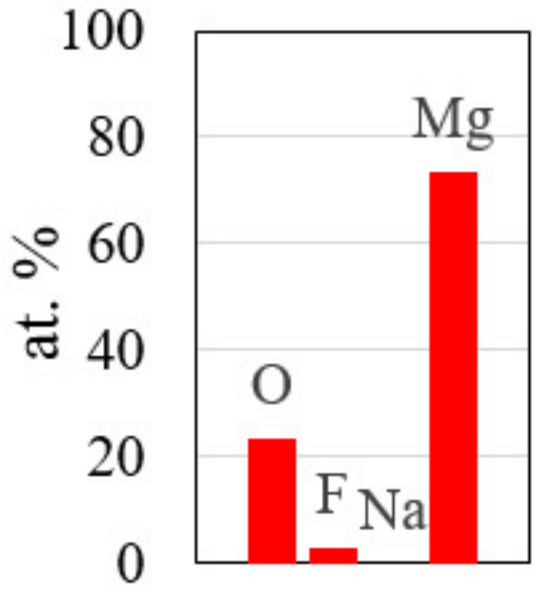

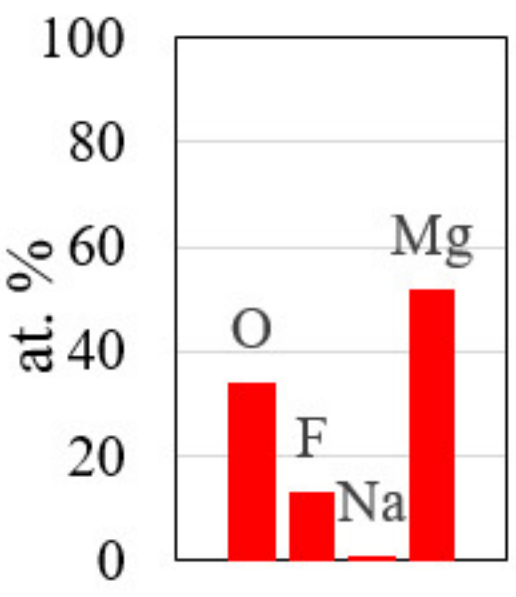

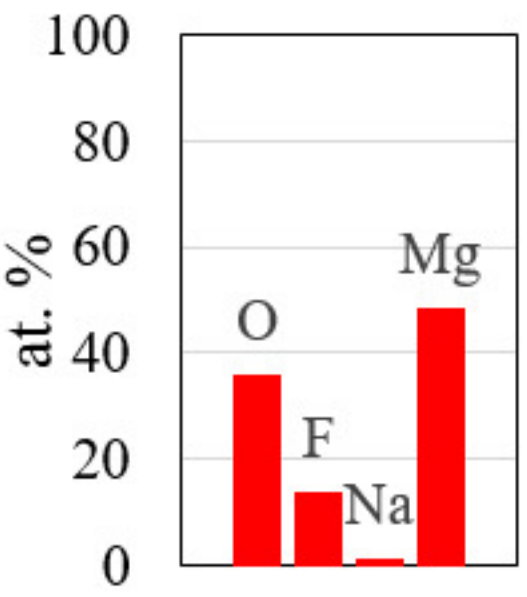

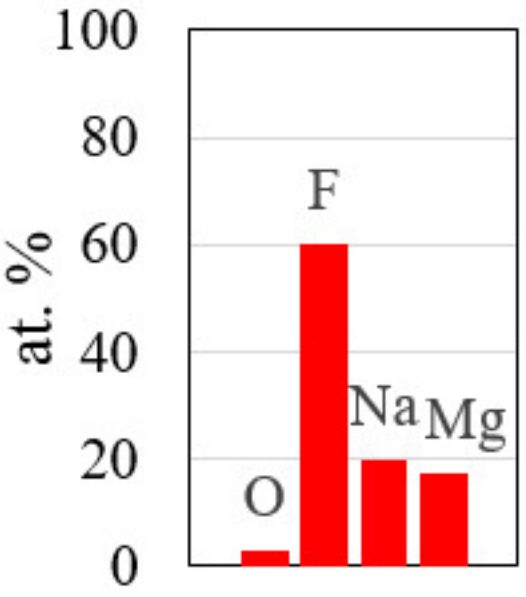

0.030 NaF

0.215 NaF

0.475 NaF

0.735 NaF

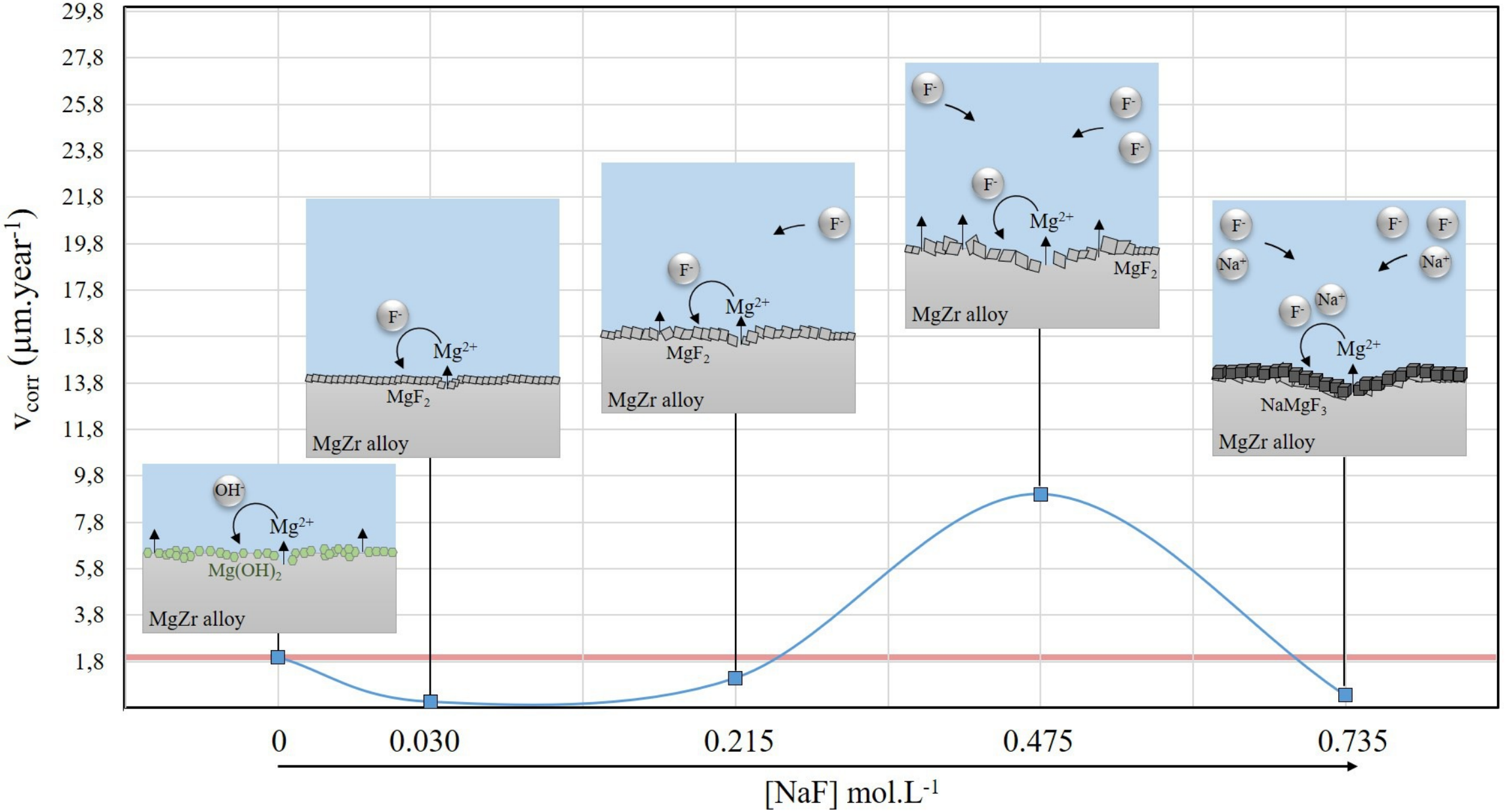
29,8
27,8
25,8
23,8
21,8
19,8
17,8
15,8
13,8
11,8
9,8
7,8
5,8
3,8
1,8
V_{corr} (µm.year^{-1})
OH$^-$
Mg^{2+}
Mg(OH)$_2$
MgZr alloy
F$^-$
Mg^{2+}
MgF$_2$
MgZr alloy
F$^-$
F$^-$
Mg^{2+}
MgF$_2$
MgZr alloy
F$^-$
F$^-$
F$^-$
Mg^{2+}
MgF$_2$
MgZr alloy
F$^-$
F$^-$
F$^-$
Na$^+$
Na$^+$
F$^-$
Na$^+$
Mg^{2+}
NaMgF$_3$
MgZr alloy
0
0.030
0.215
0.475
0.735
[NaF] mol.L^{-1}